Multi-branched model of the human arterial system

A. P. Avolio

Medical Professorial Unit, St. Vincent's Hospital, Darlinghurst 2010, Sydney, N.S.W. Australia

Abstract—*A model of the human arterial system was constructed based on the anatomical branching structure of the arterial tree. Arteries were divided into segments represented by uniform thin-walled elastic tubes with realistic arterial dimensions and wall properties. The configuration contains 128 segments accounting for all the central vessels and major peripheral arteries supplying the extremities including vessels of the order of 2·0 mm diameter. Vascular impedance and pressure and flow waveforms were determined at various locations in the system and good agreement was found with experimental measurements. Use of the model is illustrated in investigating wave propagation in the arterial system and in simulation of arterial dynamics in such pathological conditions as arteriosclerosis and presence of a stenosis in the femoral artery.*

Keywords—*Arterial branching, Arterial model, Elastic tubes, Vascular impedance, Wave reflection*

Nomenclature

ρ = blood density
c_0 = pulse wave velocity
σ = Poisson ratio for arterial wall

F_{10} = the expression $\dfrac{2J_1(\alpha j^{3/2})}{\alpha j^{3/2} J_0(\alpha j^{3/2})}$.

where J_0 and J_1 are Bessel functions of the first kind, and order zero and one, respectively, and $\alpha = R_0\sqrt{\omega\rho/\mu}$
γ = propagation constant
ω = angular frequency
E = Young's modulus of arterial wall
h = wall thickness
R_0 = internal radius of arterial segment
η_w = viscoelasticity of the arterial wall
Γ = reflection coefficient
μ = blood viscosity

1 Introduction

SINCE William Harvey established the concept of circulation of blood in 1628, numerous attempts have been made at gaining insight into the physical relationship between the forces involved in propelling blood in the complicated anatomical structure of the circulatory system. The fact that the arterial tree

transforms intermittent flow from the left ventricle to a more steady outflow was recognised by Hales in 1733. He described the arterial system as a single elastic chamber which later became known as the Windkessel model (FRANK, 1899). Although this simple concept is sometimes used in determination of cardiac output (MCDONALD, 1974), it fails to explain the phenomenon of pulse wave propagation throughout the arterial tree as the inherent property of the simple Windkessel model assumes an infinite pulse wave velocity. For a detailed analysis of the dynamics of arterial blood flow, a model is required which includes the multi-branched configuration of the arterial system, and a description of the distributed nature of arterial properties. An accurate representation is essential especially for the human arterial tree because of the numerous practical difficulties of obtaining a whole range of physical measurements *in vivo*. In developing the model described below, the systemic vasculature is divided into a multi-segment branching structure consisting of 128 arterial segments arranged according to the anatomical architecture of the human arterial tree. This configuration includes all the central vessels and principal arteries supplying the extremities with each segment having realistic dimensions and arterial properties. Peripheral branches are terminated with a resistance giving a specified reflection coefficient. The number of segments included in the model is determined by the desired accuracy in calculating pressure and flow waveforms throughout the system with the added limitation imposed by the available computer storage capacity.

2 Theoretical basis

The basic computational unit is a segment of artery which is considered as a thin-walled uniform cylindrical tube having internal viscous, elastic and inertial properties with external coupling to the surrounding tissue producing a longitudinal constraint. This representation was previously used by WOMERSLEY (1957), (McDONALD, 1974) to solve the Navier-Stokes equations for fluid flow in elastic tubes and apply the solution to pulsatile blood flow in arteries.

The characteristic impedance Z_0 of an arterial segment as derived by WOMERSLEY (1957) is

$$Z_0 = \frac{\rho c_0}{\sqrt{1 - \sigma^2}} \times (1 - F_{10})^{-1/2} \tag{1}$$

and the propagation constant

$$\gamma = \frac{j\omega}{c_0} \times (1 - F_{10})^{-1/2} \tag{2}$$

The wave velocity c_0 is defined by the Moens-Korteweg equation as

$$c_0 = \sqrt{\frac{Eh}{2\rho R_0}} \tag{3}$$

where E is the 'static' value of Young's modulus of the arterial wall.

The arterial wall is known to behave as a viscoelastic material (BERGEL, 1961) which has the property of producing a phase difference between applied force and resulting displacement. This frequency dependent property is thus described by the dynamic Young's modulus E_d (BERGEL, 1961), expressed as

$$E_d = E + j\omega\eta_w \tag{4}$$

where η_w is the wall viscosity.

With respect to pulse wave propagation, the viscoelastic properties of the arterial wall are characterised by the tangent of the angle ϕ representing the phase lead of pressure in relation to wall displacement. (TAYLOR, 1959; HARDUNG, 1962; WESTERHOF and NOODERGRAAF, 1970).

$$\phi = \tan^{-1}\left(\frac{\omega\eta_w}{E}\right) \tag{5}$$

TAYLOR (1966) derived an expression for the variation of ϕ with frequency as

$$\phi = \phi_0(1 - e^{-k\omega}) \tag{6}$$

where ϕ_0 is an asymptotic value and k was taken as 2. Hence by use of the dynamic Young's modulus, $E_d = |E| e^{j\phi}$, the equation for wave velocity becomes

$$c_0' = c_0 \times e^{j\phi/2} \tag{7}$$

i.e. $c_0' = c_0 \times (\cos(\phi/2) + j\sin(\phi/2))$

This modifies the equations for characteristic impedance and propagation constant to

$$Z_0 = \frac{\rho c_0}{\sqrt{1 - \sigma^2}} \times (1 - F_{10})^{-1/2}$$
$$\times \{\cos(\phi/2) + j\sin(\phi/2)\} \tag{8}$$

$$\gamma = \frac{\omega}{c_0} \times (1 - F_{10})^{-1/2}$$
$$\times \{\cos(\phi/2) - j\sin(\phi/2)\} \tag{9}$$

Once characteristic impedance and propagation constant are determined for the segment in terms of blood and vascular properties, input impedance, transmission ratio and phase velocity are then calculated by means of electrical transmission line theory.

If a segment of length l is terminated by an impedance Z_T, the reflection coefficient is given as

$$\Gamma = \frac{Z_T - Z_0}{Z_T + Z_0} \tag{10}$$

The input impedance of the segment (at $x = 0$) then becomes

$$Z = Z_0 \times \frac{1 + \Gamma e^{-2\gamma l}}{1 - \Gamma e^{-2\gamma l}} \tag{11}$$

and the transmission ratio of pressure at the termination ($x = l$) to pressure at the origin ($x = 0$) is

$$\frac{p(l)}{p(0)} = \frac{1 + \Gamma}{e^{\gamma l} + \Gamma e^{-\gamma l}} \tag{12}$$

The transmission ratio as given in eqn. 12 is a complex number with modulus and phase. The modulus gives the amount of amplification ($> 1 \cdot 0$) or attenuation ($< 1 \cdot 0$) of a particular frequency having travelled a length l; phase denotes the time lag, hence the time taken for that frequency to travel the length of the segment. Thus the phase velocity may then be determined from the phase angle of eqn. 12.

3 Peripheral resistance

All terminations to peripheral segments consist of a pure resistance which is determined by the nominal characteristic impedance of the segment and the specified reflection coefficient (Γ_0). The characteristic impedance Z_0 is determined from eqn. 8 and the terminal resistance R_T obtained from eqn. 10 is

$$R_T = Z_0 \times \frac{1 + \Gamma_0}{1 - \Gamma_0} \tag{13}$$

The resistance R_b due to blood viscosity for a segment of length l is determined according to Poiseuille's law as

$$R_b = \frac{8\mu l}{\pi R_0^4} \tag{14}$$

The total branch resistance for a terminal segment is $R_T + R_b$. This is then added in parallel with the resistance of other connecting branches, and working backwards towards the origin the total peripheral resistance is obtained, which is defined as the input impedance at zero frequency. It thus comprises the resistance due to peripheral terminations anatomically occuring at the arteriolar level and that owing to viscous losses throughout the arterial system.

4 Physiological data

Vascular dimensions and elastic constants for the human arterial tree were obtained from the literature; the main source being the original data compiled by NOORDERGRAAF et al. (1963) and subsequently updated by WESTERHOF et al. (1969). When the anatomical configuration described by these workers was used in this present model it was found to give an unsatisfactory representation of the vascular beds in the upper limbs and head particularly in synthesising flow waveforms in the brachiocephalic artery. While pressure and flow waveforms in the lower part of the body corresponded well with reality, flow waveforms calculated in the brachiocephalic artery varied markedly with measured flow patterns in that they did not show the shorter duration of forward flow compared to that in the ascending aorta. This characteristic brachiocephalic flow pattern has been shown to indicate earlier return of reflected waves from the upper vascular bed compared with those from the lower body both in

man and other mammals (MILLS et al., 1970; O'ROURKE 1967; AVOLIO et al., 1976). Since wave reflection in the aorta influences the hydrodynamic load presented to the left ventricle by the arterial system, it is important that vascular impedance of the major vessels close to the aortic root is faithfully simulated. Significant improvement was achieved by addition of further arterial branches in the upper part of the body. The branching configuration and relative dimensions were obtained from anatomical atlases. Segments added to the originally named configuration of Noordergraaf are shown in Table 1 marked with an asterisk. The lengths of these vessels were taken up to the major bifurcation and the wall thickness was estimated on the basis of comparable h/R_0 ratios of previously specified arteries in the same vascular bed.

The increase in pulse wave velocity due to the elastic tapering was taken into account by a progressive increase of Young's modulus from central to peripheral vessels, (WESTERHOF et al., 1969). The value for E was taken as 4×10^6 dyne/cm^2 in the central aortic region, twice this value for the legs and upper arms, and four times for the peripheral segments.

Since the significant physiological frequency range is 0–15 Hz (MCDONALD, 1974), the length of each arterial segment is taken such that the cutoff frequency is greater than 15 Hz. The cutoff frequency is determined by calculating the equivalent inductance (L) and capacitance (C) of each segment. These are calculated using the results obtained by RIDEOUT and DICK (1967) who used a discrete approximation

Table 1. Anatomical data: numbers alongside the arterial segments correspond with segment numbers in the schematic arterial tree shown in Fig. 1

	Left	Right	Length L (cm)	Radius R (cm)	Wall thickness (h cm)	$E \times 10^{-2}$ dyn/cm	f_0 (Hz)
Ascending aorta	1		4·0	1·45	0·163	4	34·7
Aortic arch	2		2·0	1·12	0·132	4	16·7
Aortic arch	5		3·9	1·07	0·127	4	36·6
Thoracic aorta	11		5·2	1·00	0·120	4	27·6
Thoracic aorta	21		5·2	0·95	0·116	4	27·8
Thoracic aorta	34		5·2	0·95	0·116	4	27·8
Abdominal aorta	50		5·3	0·87	0·108	4	27·5
Abdominal aorta	65		5·3	0·57	0·080	4	29·3
Abdominal aorta	75		5·3	0·57	0·080	4	29·3
Coeliac artery	49		1·0	0·39	0·064	4	167·8
Gastric artery	61		7·1	0·18	0·045	4	29·2
Splenic artery	62		6·3	0·28	0·054	4	28·9
Hepatic artery	63		6·6	0·22	0·049	4	29·6
Renal artery	64		3·2	0·26	0·053	4	58·4
Superior mesenteric	66		5·9	0·43	0·069	4	28·1
Gastric artery	67		3·2	0·26	0·053	4	58·4
Inferior mesenteric	83		5·0	0·16	0·043	4	42·9
Common carotid (L)	4		8·9	0·37	0·063	4	19·2

(continued)

	Left	Right	Length L (cm)	Radius R (cm)	Wall thickness (h cm)	$E \times 10^6$ dyn/cm	F_0 (Hz)
Common carotid (L)	10		8·9	0·37	0·063	4	19·2
Common carotid (L)	20		3·1	0·37	0·63	4	55·1
Common carotid (R)	12		8·9	0·37	0·063	4	19·2
Common carotid (R)	22		8·9	0·37	0·063	4	19·2
Left subclavian artery	3		3·4	0·42	0·067	4	48·6
Brachiocephalic artery	6		3·4	0·62	0·086	4	45·4
Common iliac	82	84	5·8	0·52	0·076	4	27·3
External iliac	89	92	8·3	0·29	0·055	4	21·3
*Internal iliac	90	91	5·0	0·20	0·040	16	74·1
External iliac	98	99	6·1	0·27	0·053	4	30·1
Femoral artery	104	107	12·7	0·24	0·050	8	21·1
Profundis artery	105	106	12·6	0·23	0·049	16	30·3
Femoral artery	109	110	12·7	0·24	0·050	8	21·1
Popliteal artery	111	112	9·4	0·20	0·047	8	30·2
Popliteal artery	113	114	9·4	0·20	0·050	4	22·0
Anterior tibial artery	115	118	2·5	0·13	0·039	16	181·5
Anterior tibial artery	119	124	15·0	0·10	0·020	16	24·7
Anterior tibial artery	125	128	15·0	0·10	0·020	16	24·7
Posterior tibial artery	116	117	16·1	0·18	0·045	16	25·7
Posterior tibial artery	121	122	16·1	0·18	0·045	16	25·7
*Peroneal artery	120	123	15·9	0·13	0·039	16	28·5
*Peroneal artery	126	127	15·9	0·13	0·019	16	28·5
Carotid (internal)	31	37	5·9	0·18	0·045	8	49·6
External carotid	32	36	11·8	0·15	0·042	8	26·3
*Superior thyroid artery	33	35	4·0	0·07	0·020	8	78·3
*Lingual artery	43	56	3·0	0·10	0·030	8	106·9
Internal carotid	44	55	5·9	0·13	0·039	8	54·4
*Facial artery	45	54	4·0	0·10	0·030	16	113·4
*Middle cerebral	46	53	3·0	0·06	0·020	16	159·4
Cerebral artery	47	52	5·9	0·08	0·026	16	80·0
*Opthalmic artery	48	51	3·0	0·07	0·020	16	147·6
Internal carotid	60	68	5·9	0·08	0·026	16	80·0
*Superficial temporal	73	77	4·0	0·06	0·020	16	119·6
*Maxilliary artery	74	76	5·0	0·07	0·020	16	88·6
*Internal mammary	7	15	15·0	0·10	0·030	8	21·4
Subclavian artery	8	14	6·8	0·40	0·066	4	24·7
Vertebral artery	9	13	14·8	0·19	0·045	8	19·2
*Costo-cervical artery	16	26	5·0	0·10	0·030	8	64·2
Axilliary artery	17	25	6·1	0·36	0·062	4	28·2
*Suprascapular	18	24	10·0	0·20	0·052	8	29·9
*Thyrocervical	19	23	5·0	0·10	0·030	8	64·2
*Thoraco-acromial	27	41	3·0	0·15	0·035	16	133·4
Axillary artery	28	40	5·6	0·31	0·057	4	31·7
*Circumflex scapular	29	39	5·0	0·10	0·030	16	90·7
*Subscapular	30	38	8·0	0·15	0·035	16	50·0
Brachial artery	42	57	6·3	0·28	0·055	4	29·1
*Profunda brachi	58	70	15·0	0·15	0·035	8	18·9
Brachial artery	59	69	6·3	0·26	0·053	4	29·7
Brachial artery	71	79	6·3	0·25	0·052	4	29·9
*Superior ulnar collateral	72	78	5·0	0·07	0·020	16	88·6
*Inferior ulnar collateral	80	86	5·0	0·06	0·020	16	95·6
Brachial artery	81	85	4·6	0·24	0·050	4	41·1
Ulnar artery	87	94	6·7	0·21	0·049	8	42·2
Radial artery	88	93	11·7	0·16	0·043	8	25·9
Ulnar artery	95	102	8·5	0·19	0·462	8	33·9
Interossea artery	96	101	7·9	0·09	0·028	16	58·5
Radial artery	97	100	11·7	0·16	0·043	8	25·9
Ulnar artery	103	108	8·5	0·19	0·046	8	33·9

E = Young's modulus; f_0 = cutoff frequency (see text for explanation)
* Branches added to the original configuration described by NOORDERGRAAF et al., 1963

for fluid flow in cylindrical tubes. Based on their equations, which assume a parabolic velocity profile, L and C are given by

$$L = \frac{9\rho l}{4\pi R_0^2} \qquad (15)$$

$$C = \frac{3\pi R_0^3 l}{2Eh} \qquad (16)$$

The cutoff frequency f_0 is then defined as

$$f_0 = \frac{1}{\pi\sqrt{LC}} \qquad (17)$$

Values of f_0 for each segment are listed in Table 1.

5 Computational procedure

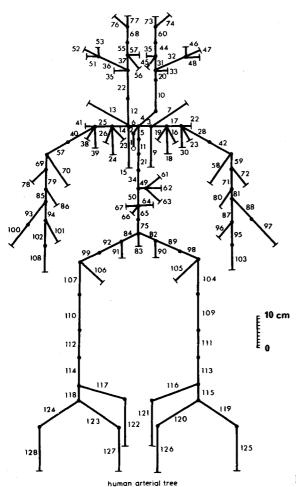A digital computer program was written in FOR-TRAN to operate on the branching configuration

shown in Fig. 1. Each segment is identified by a branch number, a node number to which it is connected and a generation number. By specifying the reflection coefficient for the terminal branches, computation is commenced from a peripheral branch continuing in a systematic order towards the aortic root. The characteristic impedance is calculated from eqn. 8 and the input impedance from eqn. 11. This is stored at the connecting node as the terminal impedance of the previous branch. Whenever there is multiple branching, the impedances are added in parallel. Transmission ratios are also stored at each node calculated from eqns. 9 and 12. By working backward towards the aortic root, the input impedance of the whole arterial tree is obtained. The final result is a complete characterisation of the branching configuration in terms of vascular impedance and transmission properties, completely specified at every node. Hence, by means of an input cardiac ejection waveform at the aortic root, pressure and flow waveforms may be determined at any node in the branching structure. Mean values of pressure and flow throughout the system are determined by peripheral resistance values obtained from terminal resistances and viscous losses in the arterial segments.

The input data to the program consist of arterial dimensions and elastic constants as shown in
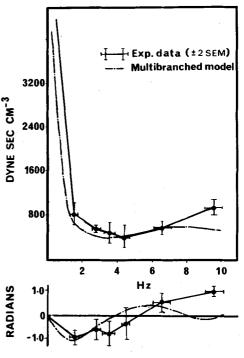

human arterial tree

Fig. 1 *Schematic representation of the human arterial tree with all lengths drawn to scale. Segment numbers correspond to arteries listed in Table 1*

Fig. 2 *Input impedance of the human arterial system. Impedance in each of the seven patients determined from simultaneous recordings of pressure and flow in the ascending aorta (Mean 2SEM). Input impedance calculated from model (broken line) at segment number 1*

Table 1, plus the following constants

Total number of segments	128
Number of nodes	68
Number of terminal segments	61
Blood density (ρ)	1·05 gm/cm³
Blood viscosity (μ)	0·04 poise
Wall viscoelasticity (ϕ_0)	15°
Poisson's ratio (σ)	0·5
Nominal reflection coefficient (Γ_0)	0·8

6 Results

6.1 Vascular impedance

Input impedance determined from the model (Fig. 2) is compared with impedance calculated from simultaneous recording of pressure and flow waves in seven patients (St. Vincent's Hospital, Sydney) during open heart surgery, immediately prior to initiation of cardio-pulmonary bypass. Informed consent was obtained from the patients and procedures were approved by the hospital. Fourier analysis of pressure and flow waves gave modulus and phase of pressure and flow components at multiples of heart rate frequency. Impedance was then determined from the complex ratio of pressure/flow as a function of frequency. (Blood flow is expressed as velocity (cm/s). This facilitates comparison of results with those of MILLS et al. (1970). Impedance modulus shows the characteristic pattern of a steep fall from the zero frequency value of 7864 dyne s cm⁻³ to a minimum at 3 Hz and a maximum at 7·5 Hz. Phase is initially negative, indicating that flow leads pressure for these frequencies. It then crosses zero at approximately the frequency values of minimum and maximum modulus. The discrepancy in the modulus between model and experimental data below 2 Hz is due to the model values being calculated at intervals of 0·5 Hz while experimental values are determined at harmonics of the normal heart rate. Although there is some variation in impedance phase of the various patients, especially at higher frequencies, all phase angles are negative below 3·5 Hz and then oscillate about zero for higher frequencies, as seen in the model calculations.

Impedance in the descending thoracic aorta and in the brachiocephalic artery determined from the model also compare favourably with measured values in these vessels. These are illustrated in Fig. 3, where the experimental data have been taken from measurements by MILLS et al. (1970). Good agreement was found both in values of modulus and phase and in the frequencies of modulus minimum and maximum and zero phase. Minimum modulus and zero phase for the descending thoracic aorta occurred around 3 Hz while that for the brachiocephalic artery was around 5 Hz. When the original configuration employed by NOORDERGRAAF et al. (1963) was used to determine impedance in the brachiocephalic artery, minimum modulus and zero phase occurred

at a frequency lower than 3 Hz. As previously described (O'ROURKE, 1967), the frequency of occurrence of minimum modulus and zero phase angle, together with wave velocity may be used to determine the distance to an effective reflecting site located downstream from the site of measurement. Considering the Noordergraaf configuration, the reflecting site for the vascular beds in the upper part of the body would be located at a greater distance relative to the aortic root than that for the lower part of the body and in fact outside the physical dimensions of the head and upper limbs. The improved branching structure, as shown in Fig. 1, places the upper reflecting site in accordance with anatomical dimensions. Using calculated values of pulse wave velocity for the descending thoracic aorta and brachiocephalic artery as 478 and 514 cm/s, respectively, the distances from the aortic root to the upper and lower reflecting sites is calculated as 25·7 cm and 39·8 cm. Considering the variation in body dimensions between that used by MILLS et al. (1970) and that used for model calculations, there is a good agreement between these values and those estimated by these workers as 29·0 and 41·0 cm, respectively. MILLS et al. (1970) calculated the lower reflecting site from the
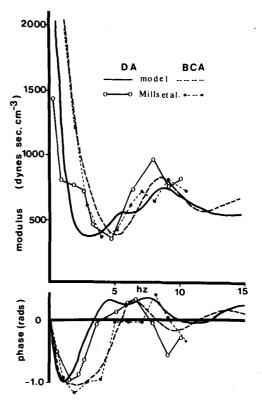

Fig. 3 *Impedance in the descending aorta (DA) and brachiocephalic artery (BCA) obtained from* MILLS *et al., (1970). Impedances determined from model for segments 11 (DA) and 6 (BCA), respectively*

seventh thoracic vertebra (T7) as 31 cm. The figure of 41·0 cm is then obtained by estimating T7 to be 10 cm away from the origin of the descending thoracic aorta.

6.2 Wave transmission and synthesis of pressure and flow waves

By using a cardiac ejection pulse as input to the model at the aortic root, pressure and waveforms may be synthesised at any node in the network by means of the calculated impedances and transmission ratios for each segment. Fig. 4 shows the pressure wave in the ascending aorta and pressure and flow in the femoral artery obtained with an input flow pulse recorded in the ascending aorta of a human subject at a heart rate of 75 beats/min. Mean and pulse pressure values are within the normal physiological range. Peak pressure in both cases occurs after peak flow as is observed in reality. The femoral pressure shows the characteristic increase in peak pressure and a loss of the incisura with a shallow diastolic wave. The time delay between the aortic and femoral wave is estimated by extrapolating the initial rise of the wave to obtain the foot-to-foot velocity as described by McDONALD (1974). A delay of 155 ms was estimated over a distance of 74·3 cm which gave an average wave velocity in the descending aorta of 480 cm/s. This agrees with the velocity calculated by the Moens-Korteweg formula for branch number 11 as 478 cm/s. The calculated flow wave in the femoral artery also shows a similar time delay. Peak velocity is reduced and prominent oscillations occur in the diastolic portion of the wave. Similar patterns were found in measurements of human femoral artery flow (LITTLE et al., 1968) as well as in dogs, (O'ROURKE and TAYLOR, 1966; McDONALD, 1974).
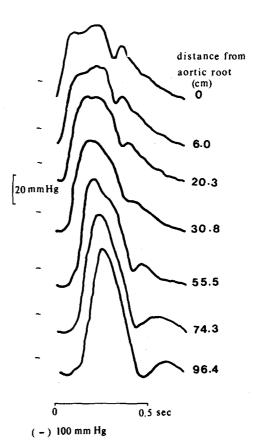

Fig. 4 *Pressure in the ascending aorta (AA; segment number 1) and pressure and flow in the femoral artery (FA; segment number 109) determined from the model. A measured ascending aortic flow wave was used as input at the aortic root. The foot-to-foot time delay of the femoral pressure pulse is 155 ms over a distance of 74·3 cm (i.e. pulse wave velocity = 480 cm/s)*

(-) 100 mm Hg

Fig. 5 *Spatial distribution of pressure waveforms showing progressive alteration of pulse contour and increased delay with increased distance from the aortic root. The 100 mmHg level for each pulse is indicated by a horizontal bar (-)*

The progressive delay and increase in pulse pressure may be seen in somewhat more detail by calculating pressure waveforms at various distances along the aorta as shown in Fig. 5. The waveform becomes smoother and steeper with increasing distance from the ascending aorta. The minimum oscillation for the diastolic part of the wave appears to occur at a distance between 20·3 and 30·8 cm from the aortic root corresponding to the region between the thoracic aorta and upper abdominal arteries. These wave patterns determined from the model are consistent with those observed in humans (MILLS et al., 1970) and other mammals (O'ROURKE, 1965).

Fig. 6 shows a comparison between flow patterns determined from the model and those measured by MILLS et al., (1970) for the descending aorta, brachiocephalic artery and right common iliac artery. The input to the model was the ascending aortic flow wave obtained from MILLS et al., (1970). The brachiocephalic flow shows a shorter duration of forward flow compared with that in the ascending and descending aorta. This is consistent with a relatively closer reflecting site in the upper part of the body than in the lower such that reflected waves return earlier. Similar brachiocephalic flow patterns have been found in dogs and other animals (AVOLIO et al., 1976).

7 Simulation of pathological arterial conditions

One of the main attributes of the arterial model based on the physiological branching configuration of the arterial tree is to be able to simulate pathological conditions such as arteriosclerosis (in the form of decreased arterial elasticity) and varying degrees of stenosis in a particular arterial segment. Other effects such as variation in peripheral vasodilation and vasoconstriction may be studied in relation to input impedance and wave transmission properties.

7.1 Arteriosclerosis

Since there is insufficient accurate information available on the variation of arterial elasticity in any particular vascular bed, no attempt was made at selective variation of elastic constants throughout the arterial tree. For the purposes of this simulation an overall increase of arterial stiffness was assumed to occur. Impedance and wave transmission calculations were carried out with the Young's modulus of all branches four times the normal value. This has the effect of doubling wave velocities since velocity is
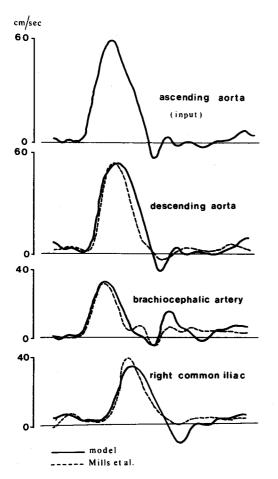

Fig. 6 Flow waves in the descending aorta (segment No. 11), brachiocephalic artery (segment No. 6) and right common iliac artery (segment No. 84). The flow pulse in the ascending aorta (input to model) and flow waveforms shown with a broken line were obtained from experimental measurements of MILLS et al., (1970)
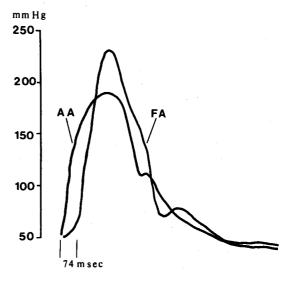

Fig. 7 Pressure in the ascending aorta (AA) and femoral artery (FA) determined from model with an input flow wave shown in Fig. 4. Magnitudes of Young's modulus (E) for all segments increased by a factor of 4

proportional to $\sqrt{E}$. From a normal cardiac ejection waveform (Fig. 4), pressure was synthesised in the ascending aorta and femoral artery as shown in Fig. 7. The characteristic 'hypertension' pattern is seen where there is an increase in peak systolic pressure, a small incisura at the end of systole and an exponential decay during diastole. The increase in pulse wave velocity is seen in the shorter foot-to-foot delay between pressure waves in the ascending aorta and femoral artery compared to pressure waves in Fig. 4.

7.2 Arterial stenosis

Simulation of arterial stenosis in the model was carried out by decreasing the radius of the segment corresponding to the femoral artery (segment 109 in the Table 1). Pressure and flow waveforms were then computed proximal and distal to the obstruction (Fig. 8). Computations were carried out with a similar input cardiac ejection wave both in the normal and stenosed state. This assumes constant values of heart rate, stroke volume, duration of ejection and cardiac output. Since these parameters are controlled by venous return and other autoregulatory mechanisms, they are not taken into account in the model. However, the above assumption is not unrealistic. In an early study of different degrees of aortic coarctation in dogs, GUPTA and WIGGERS (1951) obtained average values of 13% decrease in heart rate and 9% increase in cardiac output for 95% coarctation of the descending aorta. Since these changes are not drastic compared to the high degree of coarctation compensator mechanisms appear to be active in maintaining constant cardiac output. It thus appears to justify the use of an identical flow wave input to compare pressure and flow determined from the model with and without arterial stenosis.

Effect of progressive increased stenosis on mean pressure and proximal and distal pressure is shown in Fig. 9. Only a slight increase in mean pressure occurred up to 90% stenosis. (Percentage stenosis is
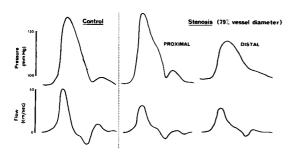
defined as $(D_0 - D_1) \times 100/D_0$, where D_0 and D_1 are the original and decreased diameter of the segment).
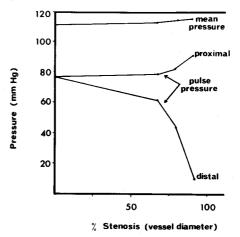
Fig. 9 *Variation of mean arterial pressure and pulse pressure distal and proximal to a stenosis in the left femoral artery*

Changes in pulse pressure, both proximal and distal, are also not great until 65% stenosis, above which there is a steep decrease in distal pulse pressure and an increase, to a lesser degree, of proximal pulse pressure. These results agree favourably with experimental measurements in dogs by GUPTA and WIGGERS (1951) reporting that about 60% aortic coarctation was required before significant changes were obtained in proximal (aortic) and distal (femoral) pulse pressures. Similar results were obtained more recently by YOUNG et al. (1975) who measured pressure drops across artificially induced stenosis in the femoral arteries of dogs.

These results indicate that a vessel such as the femoral artery can undergo a reduction in lumen diameter by a factor of 3 before obstruction is detected in either proximal or distal pressure measurements. The distributed nature of the model allows similar calculations to be done for obstructions in any vessel both central and peripheral or for graded stenosis in particular vascular beds.

8 Conclusion

A multi-branched model of the human arterial system has been constructed on a digital computer where arterial segments were represented by uniform tethered elastic tubes and characterised by electrical transmission-line properties. The model exhibits the essential features of the physical system with respect to vascular impedance and spatial distribution of pressure and flow waveforms. While the bulk of the anatomical arterial data was obtained from similar electrical analogue models (NOORDERGRAAF, 1963;

Fig. 8 *Calculated pressure and flow waveforms in the femoral artery (segment number 109) under control conditions and in the presence of a stenosis corresponding to a 79% reduction in vessel lumen diameter. Waveforms are obtained both proximally and distally to the stenosis*

WESTERHOF et al., 1969; JAGER et al., 1965) the vascular representation of the head and upper extremities was significantly improved by addition of extra branches which were of comparable dimensions to those originally described by these workers.

Although the digital computer model of the arterial system described by TAYLOR (1966) convincingly demonstrated many phenomenological aspects of the multi-branched structure of the arterial tree, it did not represent the system in terms of its physiological anatomy. This has certain associated limitations with respect to simulating arterial dynamics at specified locations. In this respect, the present arterial model may be considered an improved version of similar multi-branched arterial models constructed as digital computer simulations or as electrical analogue circuits. Perhaps an added advantage is the flexibility afforded by a digital model in terms of alterations of arterial parameters compared to its hard-wired electrical equivalent.

With a detailed representation of the human arterial vasculature, investigations on both central and regional arterial function are possible. The action of vasoactive agents may be simulated in terms of their action on peripheral resistance and their influence on pulsatile dynamics affecting ventricular load. With the increased technology in noninvasive measurement of blood flow in humans, the model may be used in parameter estimation of arterial properties associated with pathological conditions of major central or peripheral arteries.

References

AVOLIO, A. P., O'ROURKE, M. F., MANG, K., BASON, P. and GOW, B. S. (1976) A comparative study of pulsatile arterial hemodynamics in rabbits and guinea pigs. *Amer. J. Physiol.* **230**, 868

BERGEL, D. H. (1961) The dynamic elastic properties of the arterial wall. *J. Physiol.* **156**, 458

FRANK, O. (1899) Die Grundfurm des artiriellen Puls. *Zeitschrift fur Biologie.* **37**, 483

GUPTA, T. C. and WIGGERS, C. J. (1951) Basic hemodynamic changes produced by aortic coarctation in different degrees *Circ.* **3**, 17

HALES, S. (1733) 'Haemastatiks', Hafner Publishing Co., London.

HARDUNG, V. (1962) Propagation of pulse waves in viscoelastic tubings. *In* W. F. HAMILTON and P. DOWS (eds) *Handbook of Physiology, Circulation Vol. 1*, Amer. Physiol. Soc.

JAGER, G. N., WESTERHOF, N., and NOORDERGRAAF, A. (1965) Oscillatory flow impedance in an electrical analog of the arterial system: representation of sleeve effect and non-newtonian properties of blood. *Circ. Res.* **26**, 121

LITTLE, J. M., SHEIL, A. G. R., LOEWENTHAL, J. and GOODMAN, A. H. (1968) Prognostic value of intraoperative blood flow measurements in femoropopliteal bypass vein grafts. *The Lancet*, **2**, 648

MCDONALD, D. A. (1974) 'Blood flow in Arteries', (Arnold, London, 2nd edn.)

MILLS, C. J., GABE, I. T., GAULT, J. H., MASON, P. T., ROSS, J., BRAUNWALD, E. and SHILLINGFORD, J. P. (1970) Pressure-Flow relationships and vascular impedance in man. *Cardiovasc. Res.* **4**, 405

NOORDERGRAAF, A., VERDOUW, P. D. and BOOM, H. B. C. (1963) The use of an analog computer in a circulation model. *Prog. Card. Diseases* **5**, 419

O'ROURKE, M. F. (1965) 'Pressure and flow in arteries' M.D. Thesis, University of Sydney

O'ROURKE, M. F., and TAYLOR, M. G. (1966) Vascular impedance of the femoral bed. *Circ. Res.* 18 : 126

O'ROURKE, M. E. (1967) Pressure and flow waves in systemic arteries and the anatomical design of the arterial system. *J. Appl. Physiol.* **23**, 139

RIDEOUT, V. C. and DICK, D. E. (1967) Difference-differential equations for fluid flow in distensible tubes. *IEEE Trans, Biomed, Eng.* **BME-14**, 171

TAYLOR, M. G. (1959) The experimental determination of the propagation of fluid oscillations in a tube with a viscoelastic wall; together with an analysis of the characteristics required in an electrical analogue. *Phys. Med. Biol.* **4**, 63

TAYLOR, M. G. (1966) The input impedance of an assembly of randomly branching elastic tubes. *Biophys. J.* **6**, 29

WESTERHOF, N. and NOORDERGRAF, A. (1970) Arterial viscoelasticity: a generalised model. *J. Biomech.* **3**, 357

WOMERSLEY, J. R. (1957) The mathematical analysis of the arterial circulation in a state of oscillatory motion. Wright Air Development Centre, Technical Report. WADC-TR56-614

YOUNG, D. F., CHOLVIN, N. R., ROTH, A. C. (1975): Pressure drop across artificially induced stenosis in the femoral arteries of dogs. *Circ. Res.* **36**, 735